Polym. Bull. (2018) 75:4555–4569
https://doi.org/10.1007/s00289-018-2286-1

ORIGINAL PAPER

Synthesis and characterization of biofouling-resistant nanocomposites based on glucamine polymers and silver/acrylic acid nanoparticles

Manuel Palencia[1] · **Alexander Córdoba**[1,2] · **Enrique Combatt**[3]

Received: 3 October 2017 / Revised: 27 December 2017 / Accepted: 29 January 2018 /
Published online: 7 February 2018
© Springer-Verlag GmbH Germany, part of Springer Nature 2018

Abstract The objective of this work was to synthesize nanocomposites based on poly(*N*-vinylbenzyl-*N*-methyl-D-glucamine) and metallic nanoparticles, NP(VB-NMDG), from *N*-vinylbenzyl-*N*-methyl-D-glucamine (VbNMDG) and a polymerizable nanostructured crosslinker (PNC). PNC was synthesized from silver nanoparticles stabilized with acrylic acid and added to polymer phase during free-radical polymerization of VbNMDG. The boron retention properties of NP(VB-NMDG) were evaluated in function of pH and ionic strength. In addition, antimicrobial properties were evaluated against *E. coli* and *S. aureus*. Results evidenced that PNC can be synthesized by chemical reduction from Ag^+, BH_4^- and acrylic acid as stabilizing agent. In addition, PNC can be added during the polymerization reaction to obtain NP(VB-NMDG). Effect of pH on boron retention of nanostructured polymer was significant only at low ionic strength (the order seen was pH $5.0 > 7.0 > 9.0$). The ionic strength was identified to strongly decrease the boron retention by NP(VB-NMDG). Finally, NP(VB-NMDG) showed antimicrobial activity enhanced by incorporation of AgNPs.

Keywords Silver nanoparticle · Nanocomposite · *N*-methyl-D-glucamine · Boron

✉ Manuel Palencia
manuel.palencia@correounivalle.edu.co

[1] Research Group in Science with Technological Applications (GI-CAT), Department of Chemistry, Faculty of Natural and Exact Sciences, Universidad del Valle, Street 13 N° 100-00, Campus Melendez, Cali 25360, Colombia

[2] Mindtech Research Group (Mindtech-RG), Mindtech S.A.S, Cali, Colombia

[3] Department of Agricultural Engineering and Rural Development, Faculty of Agricultural Sciences, Universidad de Córdoba, Montería, Colombia

Introduction

Boron is an essential element for plants, animals and humans; in addition, boron is widely used in fiberglass insulation, borosilicate glass, metal welding, flame retardant, pharmaceutical manufacturing and is used as dopant for semiconductors [1–5]; But also, boron is a component of soils, rocks and natural waters. For plants, boron is a micronutrient required in small amounts depending on plant species, but it is characterized by a narrow range between essentiality and toxicity. For humans, amount of boron required for life is very limited and ingestion of an excess of this element produces nervous system disease [3]. According to the World Health Organization (WHO), the limiting concentration of boron in drinking water is 2.4 mg L^{-1} [1]. However, the increase of environmental pollution and health problems caused by various boron applications have been reported [1–3].

From the above, technologies for boron removal, separation and recovery from aqueous solutions are of great interest. Removal of boron from industrial waste, sea water, water for irrigation, geothermal water, ceramic or optoelectronic industries has been widely investigated [1, 2]. Also, several separation technologies, such as adsorption with inorganic adsorbents, ion exchange, solvent extraction, and reverse osmosis have been applied for the recovery of boron from aqueous solutions [3].

Recently different materials containing NMDG units have been developed for boron removal, including cellulose fibers, polyurethanes, polyols, resins based on vinylbenzyl chloride and divinylbenzene, microporous polypropylene, ultrafiltration membranes, interpenetrating polymer networks, nanocomposite resins based on montmorillonite as disperse phase, among other [4–12].

In particular, the glucamine group has been widely reported as an effective chelating group for the making of boron adsorbents (see Fig. 1a). Many researches have been centered on the use of *N*-methyl-D-glucamine (NMDG) or its derivatives

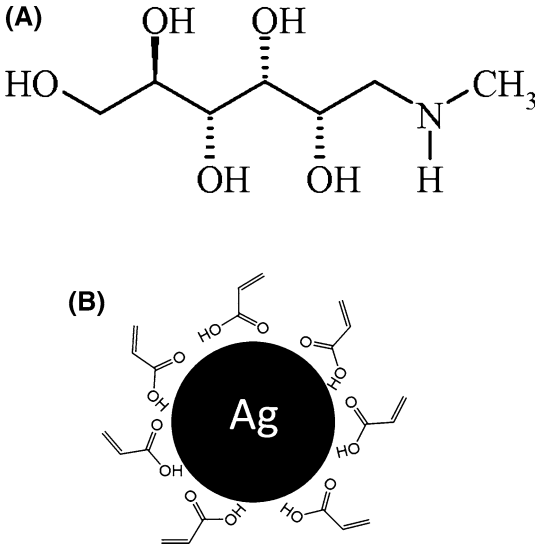

Fig. 1 **a** Structure of *N*-methyl-D-glucamine and **b** illustration of Ag–Acrylic acid nanoparticles

for the boron removal because NMDG groups can coordinate boric acid from aqueous solutions under different conditions. However, poor mechanical properties and an easy bacterial colonization are expected as a result of hydrophilic features of NMDG, and its harmlessness; in consequence, the making of new polymer materials for the development of new technologies for removal, retention and recovery of boron from aqueous solution are of great interest; thus, the use of fillers at nanometric level emerges as an alternative promising for the enhancement of polymer properties and to give greater functionality for the desired application.

It has been reported that nanofillers in the range of 3–5% by weight achieve the same reinforcement as 20–30% of microsized fillers [13]. Thus, nanocomposites have a weight advantage over micrometric composites, as well as, these offer a higher specific interfacial area enables potentially to increase the interfacial interactions with polymer phase. But also, "active" nanofillers can be used to give special properties to polymer phase, for example, antimicrobial properties from Ag^0 nanofillers. Antibacterial properties of AgNPs are well-known being suggested that AgNPs can act by two mechanisms: release of Ag^+ from AgNPs acting as reservoir or direct interaction of AgNPs with biomolecules or sites in the bacteria [14–16]. Therefore, bi-functional materials for boron removal could be obtained from nanocomposites based on a functional polymer phase with NMDG ligands and "active" nanofiller using silver nanoparticles (AgNPs).

On the other hand, recently, we reported the synthesis of AgNPs by chemical reduction with sodium borohydride and functionalized with acrylic acid, which is a polymerizable vinyl monomer (see Fig. 1b) [17]. In consequence, this nanomaterial can be used for the making of nanocomposites by free-radical polymerization because vinyl units on Ag surface are expected to promote the easy insertion of nanoparticles in the polymer phase. Thus, the objective of this work was to synthesize and characterize biofouling-resistant nanocomposites based on VbNMDG and silver nanoparticles; as well as, to evaluate their boron retention and antimicrobial properties.

Experimental section

Reagents

Silver nitrate ($AgNO_3$, Aldrich) was used as source of silver ions to carry out the synthesis of AgNPs, whereas acrylic acid (99%, Aldrich) and sodium borohydride (99%, Aldrich) were used as stabilizing and reducing agents, respectively. 4-chloromethylstyrene (Aldrich, 90%) and NMDG (Aldrich, 99.5%) were used for the synthesis of *N*-vinylbenzyl-*N*-methyl-D-glucamine (VB-NMDG) using dioxane-water mixture as solvent. *N*,*N*-Methylene-bis-acrylamide (99%, Aldrich) and ammonium persulfate (98%, Aldrich) were used as crosslinking agent and radical initiator, respectively. Boric acid was used for the preparation of borate solutions. pH of solutions was regulated using 0.1 mol L^{-1} NaOH and HNO_3 solutions. $BaCl_2$ (Merck), sulfuric acid (Merck) and Agar Tryptone Soya (Aldrich) were used for antimicrobial activity test. *E. coli* and *S. aureus* were used as test

microorganisms corresponding to Gram-negative and Gram-positive bacteria, respectively. Deionized water was used in all experiments.

Synthesis of AgNPs stabilized with acrylic acid

AgNPs stabilized with acrylic acid are named as polymerizable nanostructured crosslinker (PNC); PNC was synthesized by chemical reduction, since acrylic acid can be polymerized by free-radical polymerization and silver core of AgNPs is at nanometric level. For that, 45 mL of $AgNO_3$ (3.3×10^{-4} mol L^{-1}) and 3.0 mL of acrylic acid (0.02 mol L^{-1}) were mixed and stirred for 10 min. Later, 2.0 mL of $NaBH_4$ solution were added to the mixture (1:5 Ag:BH_4^- ratio); then, mixture was stirred for 1 h at 100 rpm. Finally, PNCs were characterized by ultraviolet–visible spectroscopy (UV–vis, Shimadzu UV-1700, PharmaSpec) and dynamic light scattering (DLS, ZetasizerNano ZS90). Nanoparticles were concentrated using a centrifuge (Hettich Universal 320R) for 5 h at 5000 rpm and 15 °C; supernatant was eliminated by decantation and precipitate was diluted to total volume of 5.0 mL [17]. In addition, transmission electronic microscopy (TEM) was performed to identify the AgNPs.

Synthesis of VB-NMDG

Synthesis of VB-NMDG has been previously published [5, 6, 9, 10]. Dioxane and water, in 2:1 volume ratio, were placed in polymerization reactor and heated until total dissolution. Later, 3.20 mL (21.9 mmol) of 4-chloromethylstyrene was dissolved in 10 mL of dioxane and slowly added to the reactor. The reaction was kept under reflux with constant stirring for 5 h. Unreacted 4-chloromethylstyrene was removed by extraction with ethyl ether and functionalized monomer (VB-NMDG) remained in the aqueous phase. Characterization of VB-NMDG was performed by crystallization.

For that, a small fraction of aqueous phases was refrigerated and VB-NMDG was crystallized, washed, and filtered with cold water. Later, monomer crystals were dried at room temperature for their characterization by nuclear magnetic resonance (H^1-NMR). The H^1-NMR spectra were recorded on a Bruker Avance 400 spectrophotometer using dimethyl sulfoxide-d_6 (DMSO) as solvent and tetramethylsilane as internal standard. Synthesis was verified by a polymerization test in water [6]. Reaction yield was gravimetrically determined.

Synthesis of P(VB-NMDG) and NP(VB-NMDG)

For the synthesis of NP(VB-NMDG), VB-NMDG (1.0 g), ammonium persulfate (29.9 mg) and *N*,*N*-methylene-bis-acrylamide (66.6 mg) were dissolved in 3.0 mL of aqueous dispersion of PNC previously synthesized. Mixture was allowed to react at 80 °C for 5 h in nitrogenous atmosphere to deactivate the polymerization inhibitor. In addition, non-nanostructured polymer, P(VB-NMDG), was synthesized at the same conditions used for synthesis of NP(VB-NMDG). Polymers were purified by diafiltration using a stirred-cell ultrafiltration unit (Amicon) and

cellulose membranes (Millipore, 10 kDa); in addition, for NP(VB-NMDG), residual silver concentration was monitored in the permeate using atomic absorption spectroscopy (AA-7000 Spectrophotometer, Shimadzu). Later, polymers were dried using an airflow oven at 80 °C. Then, polymers were ground and sieved (2 mm mesh). A scheme describing the sequence of reactions used for the synthesis of nanostructured polymer is shown in the Fig. 2.

Polymers were characterized by Fourier-transform infrared spectroscopy (FT-IR, Shimadzu, FT-IR 8400), 13-carbon nuclear magnetic resonance (^{13}C-NMR, Bruker 400 UltraShield), Surface-enhanced Raman scattering (SERS, ThermoFisher Scientific), thermogravimetric analysis (TGA, Q50-TGA TA Instruments) and differential scanning calorimetry (DSC, Discovery DSC-25, TA instruments). In addition, swelling capacity (*SC*) of NP(VB-NMDG) and P(VB-NMDG) were measured by method of tea bag [18, 19], for that, tea bag with a known mass of polymer (0.1 ± 0.0001 g) was introduced into bi-distilled water (100 mL) for 24 h. After, excess of solution is eliminated by gravity for 10 min. A blank experiment in absence of polymer was performed. All experiments were performed by triplicate. Thus, *SC* is calculated by:

$$SC = \left(\frac{w_2 - (w_1 + w_0)}{w_1}\right) - SC_0 \quad (1)$$

where w_0, w_1 and w_2 are the masses of tea bag, polymer sample and polymer-tea bag system, respectively; SC_0 is the correction of *SC* by results of blank experiment. For samples highly hydrophilic like ionic polymers or hydrogels, SC_0 is negligible compared with *SC* [18].

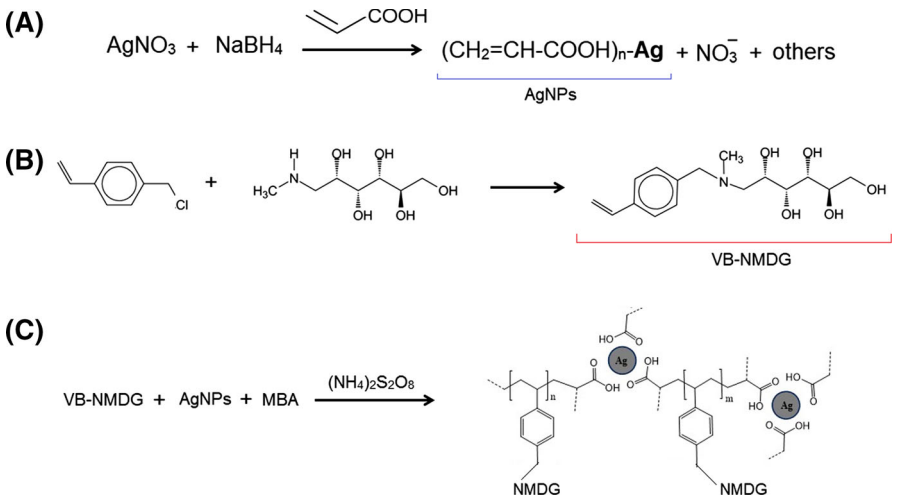

Fig. 2 Sequence of reactions used for obtaining NP(VB-NMDG): **a** synthesis of AgNPs, **b** synthesis of VB-NMDG and **c** synthesis of NP(VB-NMDG)

Study of boron retention properties of NP(VB-NMDG)

Retention properties of NP(VB-NMDG) were studied using a batch-type reactor and boric acid as target molecule. For that, NP(VB-NMDG) samples (50.0 mg) were individually placed in contact with metal ion solutions (100 mg L^{-1}) at different values of pH and ionic strength (5.0, 7.0 and 9.0 and 0.0, 0.5 and 1.5% of NaCl for pH and ionic strength, respectively). Concentration of boron was monitored over time quantified by azomethine-H method.

Evaluation of antibacterial activity

Antibacterial activity tests were performed using Tryptic Soy Broth (30 mgL^{-1} using deionized water as solvent) and two bacterial models: *E. coli* and *S. aureus*. Absorbance was measured at 625 nm and turbidity standards were prepared from barium chloride solution (0.048 mol L^{-1}) and sulfuric acid (0.180 mol L^{-1}). Colony-forming units (CFUs) were determined by McFarland scale using bacterial inoculums corresponding to 0.5 CFU mL^{-1}. Thus, 10.0 μL of bacterial dispersion was added to 5.0 mL of culture medium previously sterilized and contacted with a known mass of polymer (1.0 mg). Finally, system was incubated at 37 °C for 24 h. As blank was used NP(VB-NMDG) at the same conditions. In addition, two control experiments were performed using Ampicillin (0.50 g) as negative control and sorbitol (0.10 g) as positive control [18].

Results and discussion

Synthesis of polymerizable nanostructured crosslinker (PNC)

In Fig. 3a, b are shown the UV–vis spectra over time and the change of maximum absorbance over time for PNC dispersion. A maximum of absorbance at ∼ 400 nm corresponding to surface plasmon resonance (SPR) can be identified. In general, SPR is considered an evidence of nanostructuration of silver atoms as a result of chemical reduction being $NaBH_4$ the reducing agent [20–23]. SPR is produced by resonant oscillation of conduction electrons at the interface of nanometric particles stimulated by incident light [20]. It was observed that AgNPs were stable during the monitored time (∼ 7 days). However, a decrease of maximum absorbance was observed between first 2 days.

Synthesis of AgNPs can be described by two stages, a first stage of nucleation where "seeds" are produced and a second growth stage or aggregation where Ag^0 atom transference from aqueous phase to surface of nucleus, collisions between Ag^0 clusters, among atoms and clusters can occur [20]. According to Mie theory, if number of particles changes during growth stage then position of plasmon band must shift to longer wavelengths and, therefore, an increase in the particle size is produced [20–23]. Thus, as particle size is increased, particles are destabilized and precipitated producing a decrease of particle number in dispersion and in the intensity of maximum absorbance.

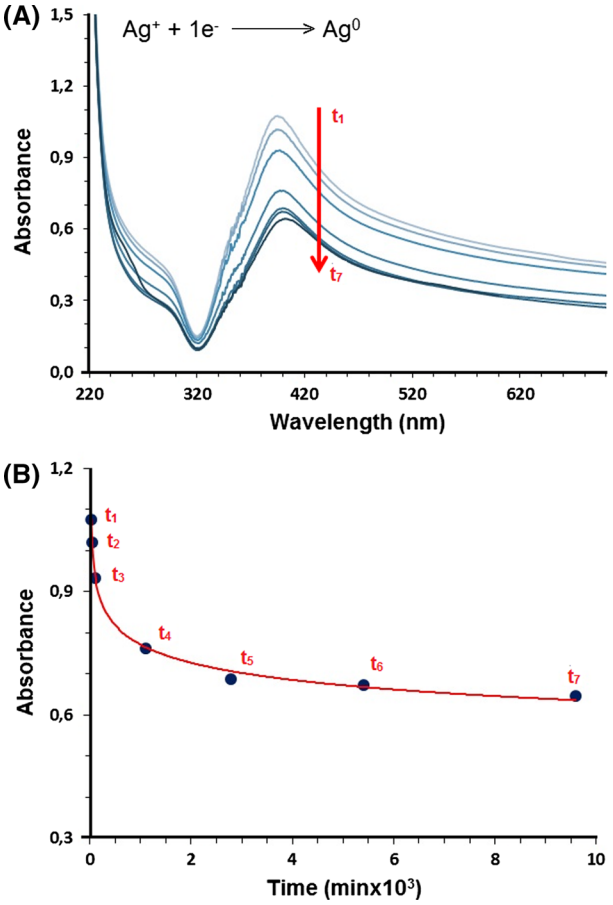

Fig. 3 **a** UV–vis spectra over time and **b** change of maximum absorbance over time for PNC dispersion

On the other hand, results of DLS are shown in Fig. 4a. It can be seen that for PNC with lower size showed values of 5.62 ± 1.61 nm in diameter. However, for PNC with larger size, observed average diameter was 111.9 ± 74.49 nm. A representative image of AgNPs obtained by TEM is shown in Fig. 4b.

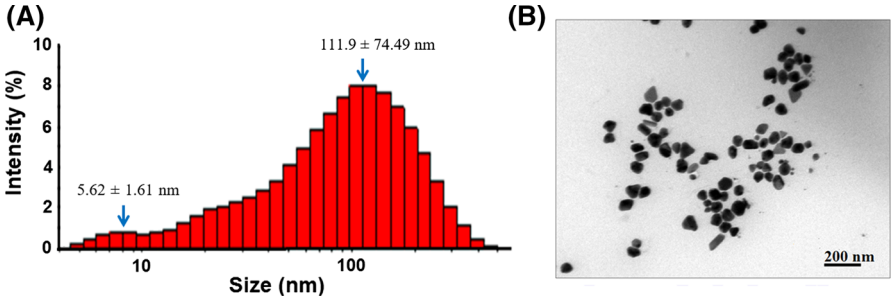

Fig. 4 **a** Size distribution of AgNPs by DLS and **b** image of TEM of AgNPs

Strategy used to synthesize the PNC was based on obtaining AgNPs stabilized by polymerizable monomers (i.e., acrylic acid). Thus, ENP is constituted by an inorganic phase (Ag^0) and organic phase. Thus, main difference between AgNPs synthesized in this work respect to those reported by other researchers is the stabilization using acrylic acid, which could permit the addition of AgNPs to polymer phase during free-radical polymerization. Stabilization of AgNPs by citric acid have been widely described [20–23], in consequence, since acrylic acid and citric acid are structurally very similar, it is suggested that when AgNPs are stabilized with acrylic acid, stabilization occurs analogously to that produced by citric acid. For synthesis of AgNPs using citrate, two different chemical species have been identified and associated with bimodal distribution observed by DLS. The first one corresponds to silver citrate and the second one is associated to "free" Ag^+ in the bulk of solution. When acrylic acid is used, bimodal distribution is also observed suggesting that two different silver chemical species are present during the synthesis by chemical reduction in aqueous solution.

Synthesis of VB-NMDG

A scheme of reaction of 4-chloromethylstyrene and NMDG is shown in Fig. 5a. In the ^{1}H-NMR spectrum (see Fig. 5b), the first signal can be identified at 2.11 ppm

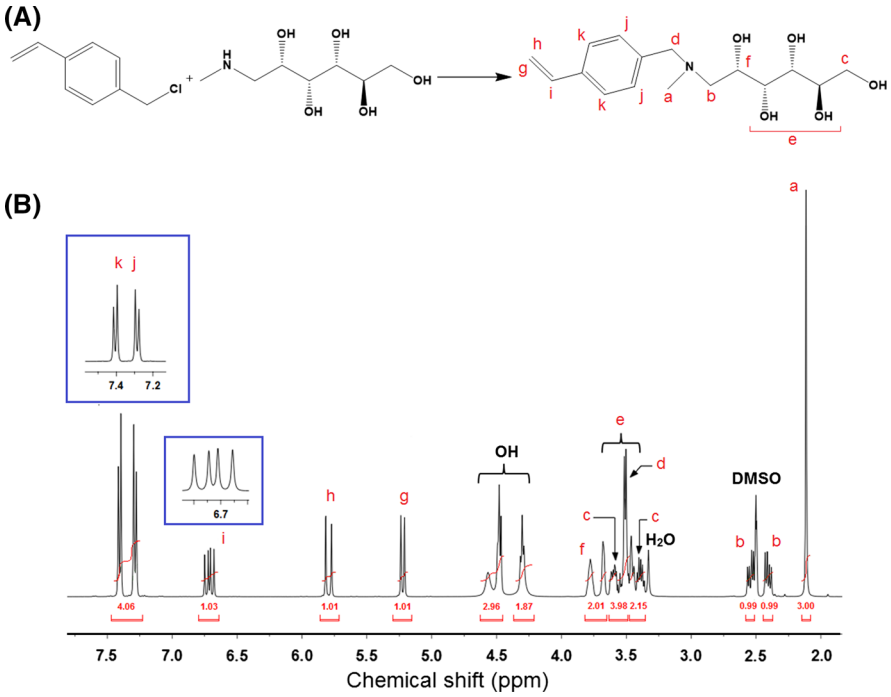

Fig. 5 **a** Scheme of reaction of 4-chloromethylstyrene and NMDG for synthesis of VB-NMDG and **b** 1H-NMR spectrum of VB-NMDG

which is integrating for three protons corresponding to methyl at 2.41 and identified as a. At 2.54 ppm, two multiplexes were attributed to the two protons of the methylene groups b and d. The protons of the carbon chain c, e and f can be attributed to the signals between 3.59 and 3.70 ppm, all signals corresponding to the protons of the hydroxyls are between 4.30 and 4.57 ppm. The doublets integrating for two protons observed at 5.23 and 5.79 ppm correspond to the proton g ($J = 11.0$ Hz) and h ($J = 17.7$ Hz), respectively, and these couple with proton i ($J = 10.9$, $J = 17.7$ Hz) which appears at 7.29 ppm. Finally, the proton signals of the aromatic ring k and j are found as two doublets at 7.29 and 7.40 ppm. The percent yield of the substitution reaction was 80.6%. In addition, the result of polymerization test was positive evidencing the presence of polymerizable double bond in aqueous phase as a result of correct functionalization of 4-chloromethylstyrene with NMDG.

Synthesis and characterization of P(VB-NMDG) and NP(VB-NMDG)

A comparison of results of characterization between P(VB-NMDG) and NP(VB-NMDG) is shown below. Spectra of FT-IR and ^{13}C-NMR are shown in Fig. 6a, b, respectively. It is observed, a great likeness between P(VB-NMDG) and NP(VB-NMDG) spectra, suggesting an evident result, polymerization was carried out correctly in both cases. From FT-IR spectra, can be identified at 3360 cm^{-1} the vibration of O–H bond, in particular, this signal is associated with acrylic acid of PNC and NMDG chains. Other signals are associated with CH_2, carbonyl group (on acrylic acid and *N*,*N*-methylene-bis-acrylamide structures) and C–N at $\sim$ 2950, $\sim$ 1650, $\sim$ 900 cm^{-1}, respectively. In addition, C=C vibration appears at $\sim$ 1620–1680 cm^{-1}.

On the other hand, the following signal were identified from ^{13}C-NMR spectra: In the range from 30 to 55 ppm signals are associated to methylene carbon, from 120 to 140 ppm signals are associated with aromatic ring, from 80 to 100 and 140–180 ppm signals are associated to C–N bonds resulting of functionalization of 4-chloromethylstyrene, and finally, also signals associate with crosslinking agent, *N*,*N*-methylene-bis-acrylamide, between 175 and 190 ppm for carbonyl group and between 75 and 90 ppm for N–C–N group were identified. In addition, among 60–90 ppm appears signals associated to units of CH_2–OH of NMDG.

Results of analysis by SERS of P(VB-NMDG) and NP(VB-NMDG) are shown in Fig. 7. It can be seen that the enhancement of signals for NP(VB-NMDG) respect to P(VB-NMDG) for lower wavenumber. SERS is based on the huge enhancement of the Raman emission of organic molecules when they are placed in the proximities of certain nanostructured metallic surfaces, in consequence, signal enhancement in the Raman spectrum can be used to identify the presence of AgNPs in the polymer phase since for it to occur, the metal nanoparticles must be small relative in comparison with the wavelength of the excitation light [24, 25]. The successful application of metal nanoparticles in SERS strongly depends on the metal characteristics, in terms of morphology (shape, size and aggregation state) and the metal nature of the nanostructured metals.

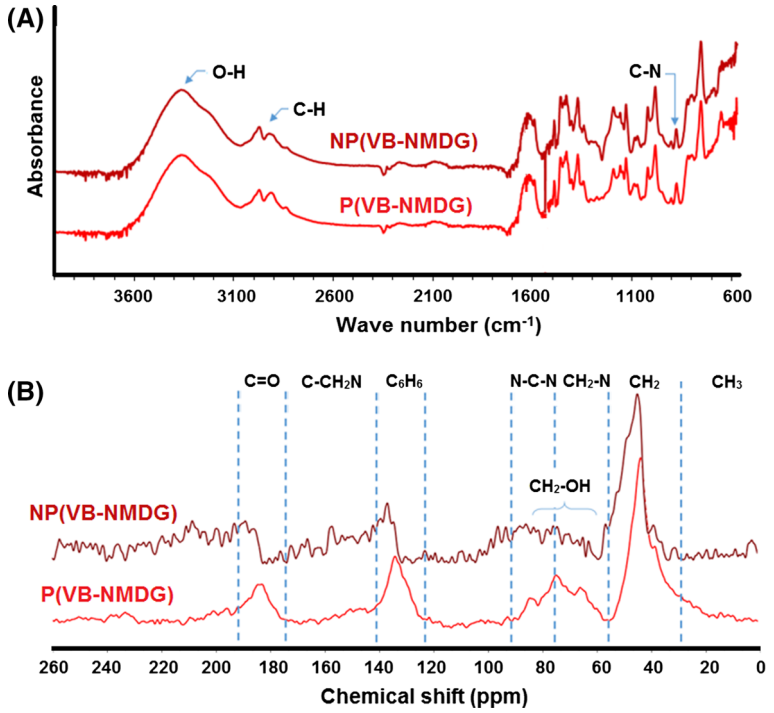

Fig. 6 **a** Spectra of FT-IR for P(VB-NMDG) and NP(VB-NMDG) and **b** spectra of 13C-NMR for P(VB-NMDG) and NP(VB-NMDG)

Results of thermal analysis [TGA, DSC and differential thermal analysis, DTA, for P(VB-NMDG) and NP(VB-NMDG)] are shown in Fig. 8. Significant changes in the thermal stabilities of P(VB-NMDG) and NP(VB-NMDG) were not observed. Three degradation stages can be identified: In the stage 1, a mass loss around $6 \pm 1\%$ at $\sim$ 100 °C can be explained as a result of adsorbed water release from hydrophilic groups; in addition, two endothermic peaks are observed from DSC. In the stage 2, a degradation with loss of mass $\sim$ 49% is observed at $\sim$ 319 °C was attributed to loss of hydroxyl groups ($\Delta H = 44.5 \pm 4.7$ J/g); and in the stage 3, decomposition of polystyrene segments was identified at 467–469 °C ($\Delta H = 7.0 \pm 0.1$ J/g) [26]. However, a total degradation was not achieved (residual mass $\sim 31 \pm 1\%$). It can be concluded that polymers, P(VB-NMDG) and NP(VB-NMDG), were thermally stable until 320 °C.

Swelling capacity of NP(VB-NMDG) compared with those of P(VB-NMDG) showed a low decrease ($\sim$ 3%). Polymers absorbed their mass in water at $\sim$ 10%. Hydrophilic nature of NMDG-based polymers is widely known and hydroxyl groups on polymer chain are the main factor to produce a favorable interaction with water molecules; however, the absence of changes of swelling capacity when synthesis is carried out in the presence of PNC suggests that a high crosslinking degree is obtained.

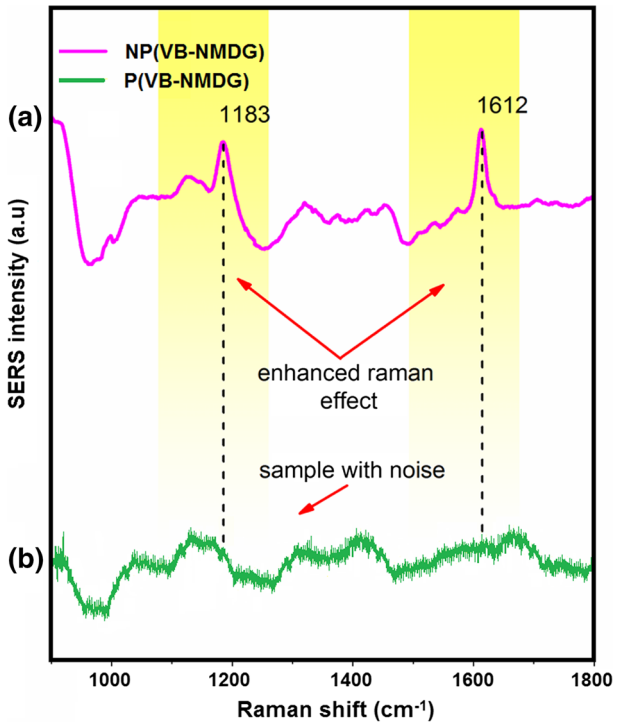

Fig. 7 SERS of P(VB-NMDG) and NP(VB-NMDG)

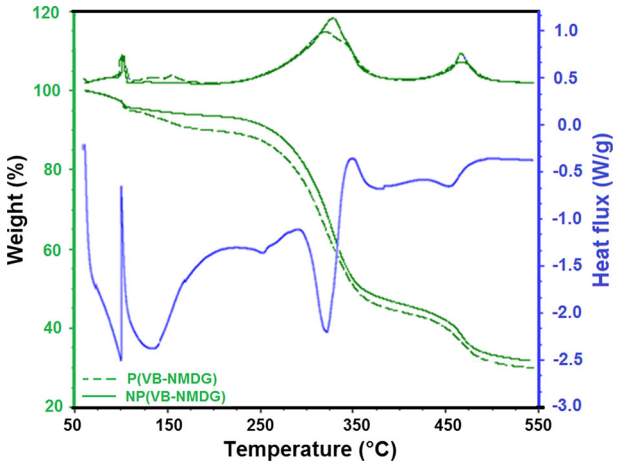

Fig. 8 Thermal analysis for P(VB-NMDG) and NP(VB-NMDG)

Boron retention by NP(VB-NMDG)

Results of boron retention by NP(VB-NMDG) are shown in Fig. 9. At 0.0% of NaCl, boron retention decreased at pH 7.0 compared with values of retention at pH 5.0 and 9.0; similar results are obtained when P(VB-NMDG) was used [6]. When ionic strength is increased (from 0.5 to 1.5% NaCl), the results evidenced the following order: $5.0 < 7.0 < 9.0$ at 0.5% NaCl (0.074 mol L^{-1}) and $5.0 > 7.0 > 9.0$ at 1.5% (0.220 mol L^{-1}) of NaCl. At low ionic strength, the greater boron retention at low values of pH can be explained by the preferential complexation of boric acid by hydroxyl groups. Boric acid is an organic acid very weak with a pK_a value of 9.2, and therefore, at low values of pH, boron acid is non-dissociated and the interaction with glucamine chains is favored, whereas at a pH greater than 10.5, it is present in the dissociated borate form and interaction with glucamine chains would be preferably by electrostatic interaction. At pH close to 9, boric acid is partially dissociated and a smaller fraction is available to be complexed by glucamine chains. For $pH < 7.0$, tertiary amine on NMDG is protonated and polymer structure is positively charged; therefore, electrostatic interaction is not favored because boron is present in a neutral form. Equilibrium reactions of boric acid species are shown in Fig. 10. However, positive charge on the polymer structure suggests that more hydrophilic structure is formed at low values of pH and, in consequence, hydration is favored and retention is increased by the flow of boron solution to inside of polymer; but also, when ionic strength is increased, two aqueous phases can be differentiated, one aqueous phase in the inside of polymer network and one aqueous phase in the outside. Thus, an increase in the salt concentration produces a greater osmotic effect counterflow in the opposite direction to the flow by hydration.

Binding mechanism of boron by NMDG chains has been described by different authors [6, 9, 10]. Boron retention by NP(VbNMDG) can be explained by the presence of available NMDG chains analogously to P(VbNMDG). Thus, NMDG groups capture boron through a covalent attachment and formation of an internal coordination complex between two hydroxyl groups in position *cis*.

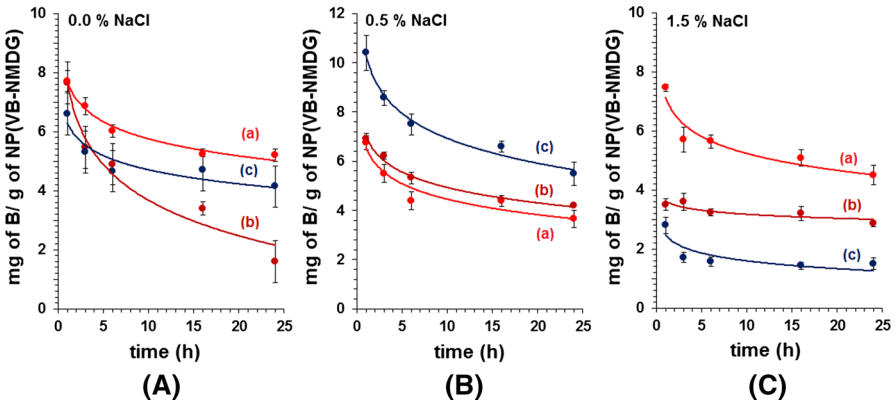

Fig. 9 Retention of Boron at different ionic strengths (0.0, 0.5 and 1.5% of NaCl) and different values of pH: **a** 5.0, **b** 7.0 and **c** 9.0

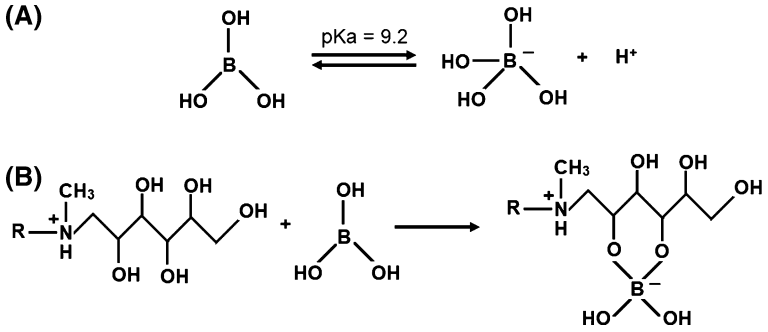

Fig. 10 **a** Dissociation of boric acid and **b** illustration of complexation of boric acid by glucamine units (R denotes the polymer chain)

Antibacterial properties of NP(VB-NMDG)

Results of evaluation of antibacterial properties of P(VB-NMDG) and NP(VB-NMDG) against *E. coli* and *S. aureus* are shown in Fig. 11. It can be seen that inhibition percentage against *E. coli* was 24%, whereas against *S. aureus* was 35% using NP(VB-NMDG). When P(VB-NMDG) was used the inhibition was lower than 10% in both cases. The increase in the antibacterial activity of NP(VB-NMDG) is explained by Ag^0 in the PNC. The mechanism of the antibacterial activity of AgNPs is complex, some authors have associated the high activity of AgNPs to that they act as a reservoir of silver ions that are released into the bacteria, interacting with the thiol groups of enzymes and proteins producing the inhibition of their functions. Other authors believe that nanoparticles can modulate signal transduction between bacteria stopping their growth, and finally, other authors have proposed that the formation of free radicals by nanoparticles can damage the cell membrane and make it porous [14–16].

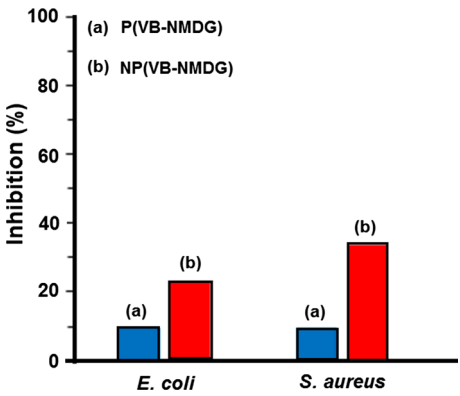

Fig. 11 Antibacterial properties of P(VB-NMDG) and NP(VB-NMDG) against *E. coli* and *S. aureus*

Conclusions

PNC can be synthesized by chemical reduction from Ag^+, BH_4^- and acrylic acid as stabilizing agent. PNC can be incorporated to P(VB-NMDG) structure by free-radical polymerization of VB-NMDG to obtain NP(VB-NMDG). Effect of pH on molybdate retention properties of NPVBtEA was significant only to null increase of ionic strength (pH 5.0 > 7.0 > 9.0). The ionic strength was identified to strongly decrease the molybdate retention by NPVBtEA. Retention results suggest that the electrostatic interaction is the main interaction influencing the molybdate retention. NPVBtEA showed antimicrobial activity enhanced by incorporation of PNC based on AgNPs.

Acknowledgements Authors thanks to Universidad del Valle and Mindtech S.A.S. for funds from projects C.I. 71050 and MT-RG project no MT-RG 002-2016.

References

1. Guan Z, Lv J, Bai P, Guo X (2016) Boron removal from aqueous solutions by adsorption—a review. Desalination 383:29–37
2. Mahmoud M, Nallappan M, Ujang Z (2014) Polymer-based chelating adsorbents for the selective removal of boron from water and wastewater: a review. React Funct Polym 85:54–68
3. Wolska J, Bryjak M (2013) Methods for boron removal from aqueous solutions—a review. Desalination 310:18–24
4. Gazi M, Galli G, Bicak N (2008) The rapid boron uptake by multi-hydroxyl functional hairy polymers. Sep Purif Technol 62:484–488
5. Palencia M, Lerma L, Córdoba A (2016) Polyurethanes with boron retention properties for the development of agricultural fertilization smart systems. J Sci Technol Appl 1:39–52
6. Palencia M, Restrepo D, Combatt E (2016) Functional polymer from high molecular weight linear polyols and polyurethane-based crosslinking units: synthesis, characterization, and boron retention properties. J Appl Polym Sci 133:43895
7. Samatya S, Ali Tuncel S, Kabay N (2015) Boron removal from RO permeate of geothermal water by monodisperse poly(vinylbenzyl chloride-co-divinylbenzene) beads containing *N*-methyl-*d*-glucamine. Desalination 364:75–81
8. Zhang X, Wang J, Chen S, Bao Z, Xing H, Zhang Z, Su B, Yang Q, Yang Y, Ren Q (2017) A spherical *N*-methyl-*d*-glucamine-based hybrid adsorbent for highly efficient adsorption of boric acid from water. Sep Purif Technol 172:43–50
9. Palencia M, Vera M, Combatt C (2014) Polymer networks based in (4-Vinylbenzyl)-*N*-methyl-*D*-glucamine supported on microporous polypropylene layers with retention boron capacity. J Appl Polym Sci 131:40653
10. Palencia M, Vera M, Rivas B (2014) Modification of ultrafiltration membranes via interpenetrating polymer networks for removal of boron from aqueous solution. J Membr Sci 466:192–199
11. Nishihama S, Sumiyoshi Y, Ookubo T, Yoshizuka K (2013) Adsorption of boron using glucamine-based chelate adsorbents. Desalination 310:81–86
12. Urbano B, Rivas B, Martinez F, Alexandratos S (2012) Water-insoluble polymer–clay nanocomposite ion exchange resin based on *N*-methyl-*D*-glucamine ligand groups for arsenic removal. React Funct Polym 72:642–649
13. Bhattacharya M (2016) Polymer nanocomposites—a comparison between carbon nanotubes, graphene, and clay as nanofillers. Materials 9:262–298
14. Palencia SL, Buelvas AM, Palencia M (2015) Interaction mechanisms of inorganic nanoparticles and biomolecular systems of microorganisms. Curr Chem Biol 9(11):23
15. Kango S, Susheel K, Celli A, Njuguna J, Habibi Y, Kumar R (2013) Surface modification of inorganic nanoparticles for development of organic–inorganic nanocomposites—a review. Prog Polym Sci 38:1261–1332

16. Palencia M, Berrio ME, Palencia SL (2017) Effect of capping agent and diffusivity of different silver nanoparticles on their antibacterial properties. J Nanosci Nanotechnol 17:1–8
17. Córdoba A, Palencia M (2017) Development of nanostructured crosslinkers with antimicrobial properties for free-radical polymerization. J Sci Technol Appl 2:54–64
18. Palencia M, Mora MA, Palencia SL (2017) Biodegradable polymer hydrogels based in sorbitol and citric acid for controlled release of bioactive substances from plants (polyphenols). Curr Chem Biol 11:36–43
19. Hosseinzadeh H (2013) Synthesis and swelling properties of a poly(vinyl alcohol)-based superabsorbing hydrogel. Curr Chem Lett 2:153–158
20. Buhro WE, Richards VN, Rath NP (2010) Pathway from a molecular precursor to silver nanoparticles: the prominent role of aggregative growth. Chem Mater 22:3556–3567
21. Gutierrez L, Aubry C, Cornejo M, Croue JP (2015) Citrate-coated silver nanoparticles interactions with effluent organic matter: influence of capping agent and solution conditions. Langmuir 18:8865–8872
22. Park K, Tuttle G, Sinche F, Harper SL (2013) Stability of citrate-capped silver nanoparticles in exposure media and their effects on the development of embryonic zebrafish (*Danio rerio*). Arch Pharm Res 36:125–133
23. Gorham J, MacCuspie R, Klein K, Fairbrother D, Holbrook R (2012) UV-induced photochemical transformations of citrate-capped silver nanoparticle suspensions. J Nanopart Res 14:1139–1155
24. Kolwas K, Derkachova A, Shopa M (2009) Size characteristics of surface plasmons and their manifestation in scattering properties of metal particles. J Quant Spectrosc Radiat Transfer 110:1490–1501
25. Mei L, Lu Z, Zhang X, Li C, Jia Y (2014) Polymer–Ag nanocomposites with enhanced antimicrobial activity against bacterial infection. ACS Appl Mater Interfaces 6:15813–15821
26. Cheng Y, Chensi X, Linling M, Scott K (2011) A polytetrafluoroethylene porous membrane and dimethylhexadecylamine quaternized poly (vinyl benzyl chloride) composite membrane for intermediate temperature fuel cells. J Power Sources 21:691–695